Influence of Structural Feature of Aluminum Coatings on Mechanical and Water Barrier Properties of Metallized PET Films

Géraldine Garnier,[1,2] Bernard Yrieix,[3] Yves Brechet,[1] Lionel Flandin[2]

[1]*Grenoble-INP, SIMAP, BP75, 1130 rue de la piscine, Saint Martin d'Hères 38402, France*
[2]*Université de Savoie, LMOPS, UMR CNRS 5041, Bât IUT, Le Bourget du Lac 73376, France*
[3]*Les Renardières, EDF R&D, Moret sur Loing F77250, France*

Received 3 April 2009; accepted 30 August 2009
DOI 10.1002/app.31372
Published online 2 November 2009 in Wiley InterScience (www.interscience.wiley.com).

ABSTRACT: This article focuses on description and evaluation of multilayer films, which are used for vacuum insulation panels (VIP). The materials investigated include a neat polyethylene terephthalate (PET) and PET films coated by chemical vapor deposition with different aluminum thicknesses. The aim of these investigations was to evaluate the influence of structural features on the physical properties of Al/PET systems. The morphological analyzes associated to water vapor permeability measurements showed that the metallized surface exhibited defects through which a small amount of water vapor can permeate. It is shown that the permeance varies linearly with the surface fraction occupied by pinholes which in turn changes linearly with the aluminum thickness. © 2009 Wiley Periodicals, Inc. J Appl Polym Sci 115: 3110–3119, 2010

Key words: aluminum coating; structural defects; metallized PET film; mechanical properties; water barrier properties

INTRODUCTION

The most critical component of a vacuum insulation panel (VIP) is the envelope, which is responsible for preventing gas and water molecule from breaking the vacuum. It is well-known that sustainable efficient barriers can be achieved with massive metal layers with a thickness of about 10 μm.[1] To avoid the degradation of the thermal properties, the thickness of the Al barrier layers should however be reduced by more than an order of magnitude. In recent year, the common way proposed to achieve ultrabarrier properties with thin films is the association of alternating inorganic layers with high intrinsic barrier properties and organic intermediate layers.[2] However, the permeation of gases (oxygen, carbon dioxide) and water vapor through coating films still represents an important problem for relatively small VIP and for regions with a climate that is warm and humid in their use as efficient barrier materials. To overcome this problem, oxide thin coatings on polymer substrates, mainly used for food and medical packaging, have been studied by a number of workers.[3–5] These studies mainly showed that oxide coatings are characterized by the presence of defects which control the oxygen and water vapor permeability of the coated film. Comprehensive knowledge of the barrier mechanisms is thus required to select the most appropriate material. For this purpose, this paper is divided in three sections:

i. A short survey of different methods used to measure aluminum thickness of polymer films is presented, then observations of coating surface are analyzed.
ii. The influence of structural features, mainly aluminum thickness and pinholes, on the physical properties is discussed.
iii. A multilayer product is analyzed to better understand how the defects could be formed in the case of commercial structures.

Correspondence to: L. Flandin (Lionel.Flandin@univ-savoie.Fr).

Contract grant sponsor: ANR (French Agence Nationale de la Recherche) BARISOL Prebat Project ADEME (Agence De l'Environnement et de la Maîtrise de l'Energie, French Agency for Environment and Energy Management).

MATERIALS AND METHODS

Materials

A biaxially oriented PET film of 12 μm thickness was used as the base material in this study. The thin barrier layers, supplied by the Rexor company

TABLE I
Designation and Characteristics of the Specimens Used

Films	Abbreviations	Aluminum thickness (nm)	Schematic representation
PET reference (12 μm of thickness)	PET12 μm	–	
PET metallized on one side with 20 nm of aluminum	PETM1F200	20	
PET metallized on one side with 30 nm of aluminum	PETM1F300	30	
PET metallized on one side with 40 nm of aluminum	PETM1F400	40	
PET metallized on one side with 80 nm of aluminum	PETM1F800	80	
PET metallized on two sides with 40 nm of aluminum	PETM2F400	2 × 40	

(at 38,850 Paladru, France) were produced by vacuum evaporation coating on to the PET film. A primary vacuum then a secondary vacuum until 4×10^{-4} mbar were used. Different aluminum (A5, 99.5%) thicknesses were deposited on the PET to investigate the influence of the aluminum layer. The maximum aluminum thickness was 80 nm, either evaporated on one side (1×80 nm) or on two sides (2×40 nm). The characteristics of all materials that are relevant to the present work are listed in Table I.

Characterization of metallized PET film

Structure examination (to study structural properties)

The scanning electron microscope used was a ZEISS Ultra 55 SEM with X-ray microanalysis (CMTC, Consortium des Moyens Technologiques Communs, located near Grenoble, France). Two different types of SEM observations were performed.

i. SEM was used to investigate the aluminum thickness on the coated films. The specimens were impregnated with an epoxy resin (EpoFix, EPOES) from Struers. The surface was polished with a RotoPol-31 polishing machine from Struers and carbon coated to prevent an accumulation of electrostatic at the surface during the SEM analysis. The preparation protocol adopted uses paper types with particle size to 68 μm until 0.75 μm. SEM images were obtained both in secondary electrons mode and back scattered electrons mode with accelerating voltages in the range of 10 to 15 kV. ImageJ software[6] was used for a micrographs treatment in an "8-bit" mode. In addition, energy dispersive (ED) technique was employed to estimate the elemental composition of an area of interest. In the case of a backscattered electrons analysis, the contrast in the image produced is determined by the atomic number of the elements in the sample. An identification of the chemical nature can also be performed especially to separate organic from metallic substances.
ii. To characterize surface fraction occupied by pinholes, the samples were analyzed on their metallized side at low accelerating voltage (4 kV) to avoid a surface degradation by electron beam. In this case the aluminum layer provided enough conductivity for the observation, and no further coating was needed. The detection of defects in an opaque coating can directly be performed by SEM secondary electron observation. Microscopy technique is thus combined with image analysis to quantify size and number of pinholes in the aluminum layer. A binary method in greyscale is employed with the help of ImageJ software to distinguish each pinhole separately (Fig. 1).

Electrical resistivity (electrical properties)

Measurements were performed using two different apparatus (i) an ohmmeter Chauvin Arnoux CA 5220 and (ii) a Keithley 237 capable of sourcing and measuring voltage or current simultaneously. The films were cut in rectangular form with a length L and a width W equal to 1000 mm and 50 mm, respectively. Copper contacts connected to electrodes of ohmmeter or Keithley apparatus were deposited on their ends to ensure a good electrical conduction. In agreement with the literature,[7] an equivalent circuit for the sample resistance in series with the contact resistance by using two-point transmission line method (TLM) was used. The determination of the aluminum thicknesses deposited on PET films was then performed thanks to (1).

$$e = \frac{L \times 315}{W \times R} \quad (1)$$

where L: length (mm); W: width (mm); R: resistance (Ω); e: thickness (Å); $\alpha = 315$ ΩÅ: resistivity

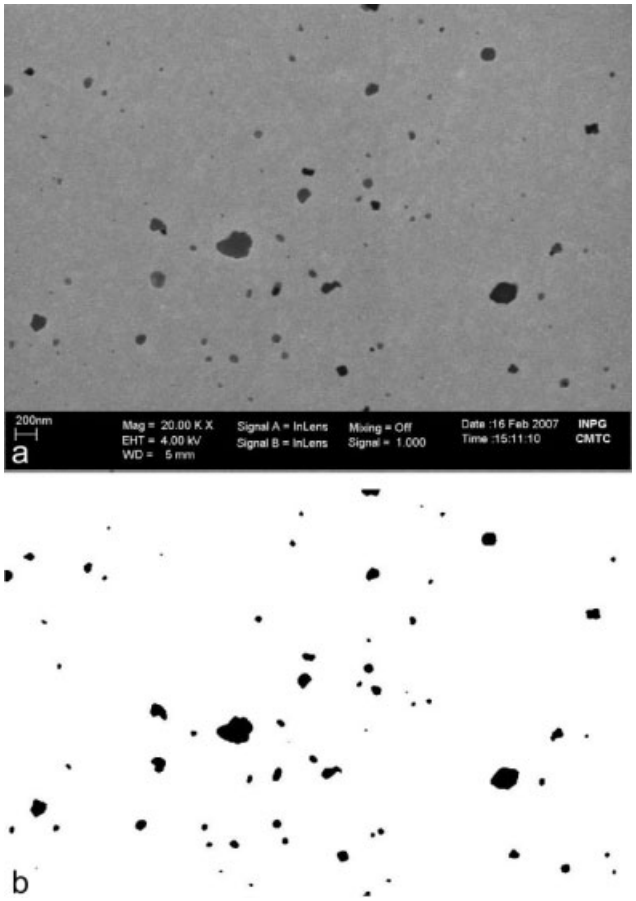

Figure 1 a) SEM secondary electron image of PETM1F200 film (b) The same image treated with ImageJ by a binary mode.

coefficient for thin layer aluminum was provided by Rexor company. A somewhat lower resistivity value 270.9 ΩÅ is reported in literature for aluminum (99.99%) at 25°C.[8] The latter value however corresponds to a bulk.

Resistance values could be directly read on the ohmmeter apparatus. For measurement with Keithley, current-voltage behavior was measured through the film thickness to determine the resistance; an ohmmic behavior of films was evidenced in all instances [Fig. 2(a)]. The contact resistances between the electrodes and the samples could be measured by varying the distance between the electrodes Figure 2(b).

Mechanical testing (to study mechanical properties)

The materials studied were oriented in two directions before coating, the direction of extrusion (machine direction, MD) and the perpendicular one transverse direction (TD). The relative amount of draw ratios determines the anisotropy in mechanical properties.[9] Tensile tests were performed following the NF ISO 6239 dumb-bell specimens, cutting the sample in both draw directions. An Adamel Lhomargy universal testing machine equipped with a 100N load cell and a grip-to-grip separation of 60 mm was used. All tests were performed at a crosshead speed of 50 mm/min. In addition, PET samples were tested at different crosshead speed, 5, 50, and 100 mm/min. From a total of at least three specimens for each test, the average values of the tensile energy to fracture E_R(kJ/m^3) which corresponds to the area under the curve were calculated.

Water vapor permeability (water barrier properties)

The "cup method" was used to measure the water permeability of the films following a procedure.[10] The mass flux through the sample is caused by creating a controlled and constant difference of relative humidities on both sides of the films. From each coated film with different aluminum thicknesses, at least three circular test specimens (110 mm in diameter) were used for vapor permeance tests (Fig. 3).

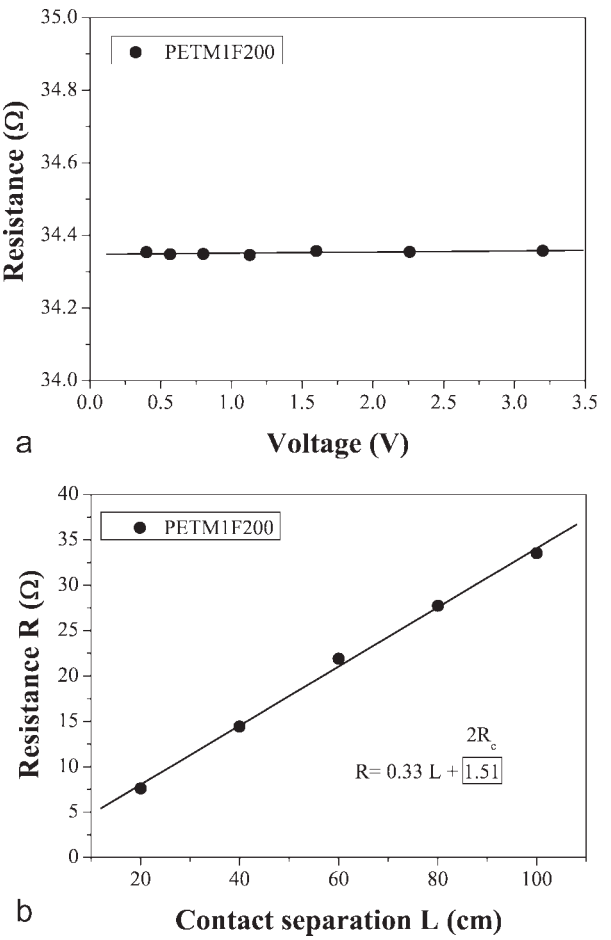

Figure 2 PETM1F200 film (PET12 μm, Al: 20 nm on one side) (a) Example of variation of the resistance with the voltage for the metallized films. (b) Determination of the contact resistance.

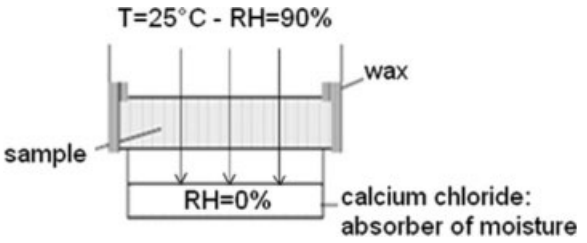

Figure 3 Schematic representation of perm cups used to determine the permeability of the films to the vapor of water.

The cups were placed in an automatic box with temperature ($T = 25°C$) and relative humidity (RH = 90%) control. This automatic system allows to store simultaneously five cups and to measure the mass of each cup typically every hour during a few days. The gain in mass of each cup is accurately measured as a function of time. A standard mass ($m = 187.507$ g) was also measured as control in each series of measurement to asses that the scale's measurements remain accurate during the test. In addition, it was also verified with a wax film that the mass transfer through it is smaller than the measurement error in the mass transfer through the film.

Water vapor permeance is defined as the time rate of water vapor transmission through unit area of flat material or construction induced by unit vapor pressure difference between two specific surfaces, under specified temperature and humidity conditions.[1] As a result, the permeance Π (kg/s m^2 Pa) can be estimated by the eq. (2):

$$\Pi = \frac{g}{S \times \Delta P} \quad (2)$$

where g: vapor flow (kg/s) calculated starting from the slope of the curve's mass variation in versus of time; S: surface test-tube (m^2); ΔP: difference of water vapor pressure (Pa), $\Delta P \sim 2500$ Pa in the present study.

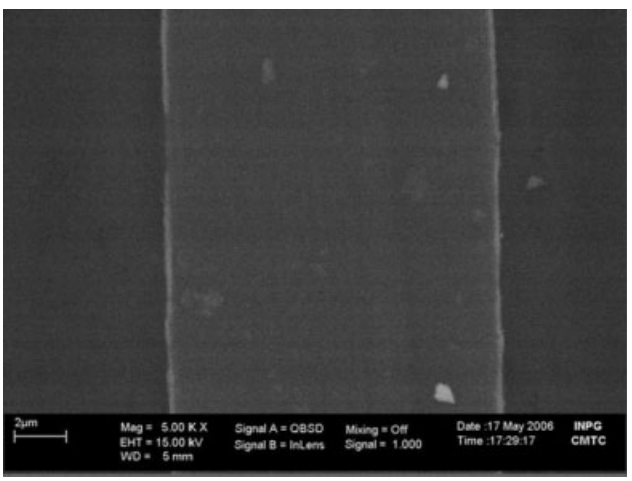

Figure 4 SEM backscattered electron micrograph of the structure of PETM2F400 film. Original magnification = 500×, marker = 2 µm.

RESULTS AND DISCUSSION

Structural features

Aluminum thickness

In a previous study, Chatham[3] measured coating thicknesses by X-ray fluorescence, calibrated by chemical analysis, multiple beam interferometry, electrical resistance measurements, and X-ray diffraction line broadening. In the present work, three coated films have been investigated by different methods, i.e. SEM and electrical resistance measurements, for a determination of the effective thickness of the aluminum layer. Figure 4 shows a SEM backscattered electron micrograph of the cross section of a PET metallized on two sides with 40 nm of aluminum. Area consisting of carbon (C) appears much darker on the gray scale than an area containing aluminum (Al); so, the thin metallic layers are easily recognizable as bright lines.

The experimental results obtained by means of different techniques were compared with those given by the supplier (Fig. 5, Table II). In the latter case, the measurements were performed with a CdA 651 ohmmeter and the contact resistances were neglected. It appears that the aluminum thicknesses may be slightly different between two sides of a given sample. SEM analysis is a reliable technique to identify components in our multilayer structures. However, it is likely that the conventional methods used for SEM samples preparation are not appropriate to determine so thin dimensions (Al < 100 nm). Since pure aluminum is very soft, mechanical cutting and polishing lead to a spreading of aluminum layers. Brunner et al.[11] recommend to use focused

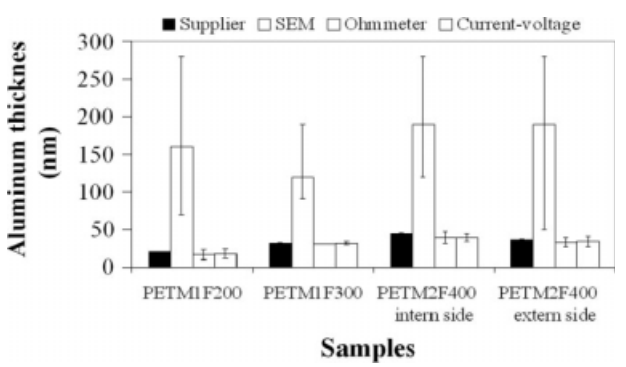

Figure 5 Aluminum thicknesses determined by SEM, Ohmmeter and current-voltage methods for three polymer-metal model films. PETM1F200: Al = 20 nm; PETM1F300: Al = 30 nm. PETM2F400: Al = 40 nm.

TABLE II
Results of Aluminum Thicknesses Determined by SEM, Ohmmeter and Current-Voltage Analyses

Samples	PETM1F200	PETM1F300	PETM2F400 intern side	PETM2F400 extern side
Film thickness supplier (μm)	12% ± 5%	12% ± 5%	12% ± 5%	12% ± 5%
Al thickness supplier (nm) [A]	19.9 ± 0.5	31.8 ± 1.0	44.7 ± 1.0	36.2 ± 1.0
Al thickness (nm) SEM [B]				
Min	70	90	120	50
Mean	160	120	190	190
Max	280	190	280	280
Error (%) [A]/[B]	>100%	>100%	>100%	>100%
Al thickness (nm) (Ohmmeter) [C]	16.5 ± 7.0	30.5 ± 1.0	39.4 ± 8.0	32.6 ± 6.0
Error (%) [A]/[C]	21	4	13	11
Al thickness (nm) U(I) [D]	17.9 ± 6.0	31.9 ± 2.0	39.4 ± 5.0	34.2 ± 7.0
Error (%) [A]/[D]	11	1	13	6

ion beam (FIB) to prepare the samples and overcome this problem. This point will be described later on in this manuscript. Electrical resistance measurements seem however to be a fast and accurate way to determine the thickness of these metallic layers. The differences between the measured values and the ones provided by the supplier remain below 10%. In addition, the experimental results show, as expected, reasonable specific contact resistances, namely 0.75 Ω and 0.43 Ω for PETM1F and PETM2F400, respectively. The measurement error due to contact resistance for the determination of aluminum thicknesses is below 5%, i.e. 2 nm. In conclusion, any electrical measurement is an extremely effective tool in the determination of aluminum thickness with sufficient accuracy when the metallic layer is applied on the external side of the film.

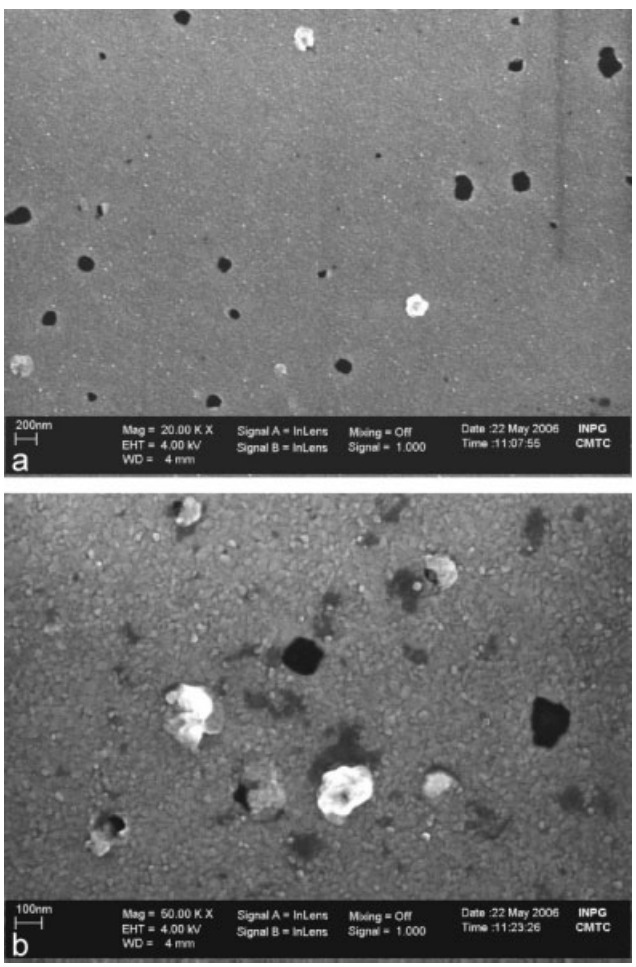

Figure 6 SEM secondary electron images of the heterogeneities present on the metallic layer of PETM2F400 film at two magnifications (a) ×20,000, (b) ×50,000.

Heterogeneities

The coated side of metallized film was examined by electronic microscopy at various magnifications. An inspection of aluminum coatings at high magnification (Fig. 6) evidences the presence of two types of heterogeneities that appear as white and black zones both with pseudo circular shapes. ED X-ray analysis permitted to estimate the elemental composition of heterogeneities. Results show that white zones contained large amounts of aluminum contrary to dark zones which were mainly organic (Fig. 7). So, white

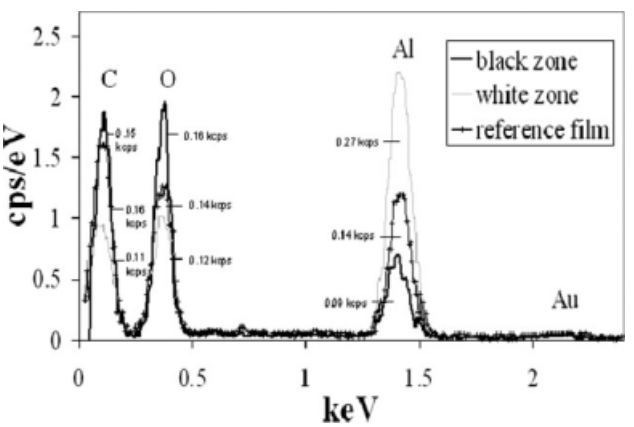

Figure 7 SEM/ED spectrum of the black and white zones present in coating; C = carbon, O = oxygen, Al = aluminum, Au = gold.

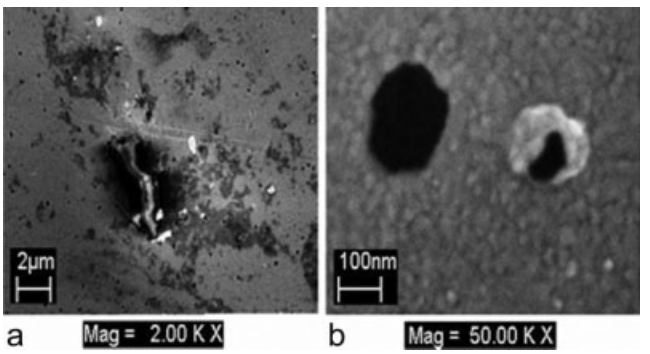

Figure 8 SEM secondary electron images of the heterogeneities present on the metallic layer of PETM2F400 film at two magnifications (a) ×2000, (b) ×50,000. EHT = 4KV, WD = 4 mm.

zones would be identified as aluminum rich phase, either heterogeneous aluminum deposition, or more likely, alumina particles. Dark spot could also be identified as pinholes in the aluminum layer.

The studies realized by Singh et al.[12] and Roberts et al.[13] report that the thin inorganic coatings present a lattice disorder with "nano-defects" and "macro-defects" resulting from the deposition process. According to these authors, nano-defects (<1 nm) result from the out-of-equilibrium growth mechanisms, while macro-defects (>1 nm) comprise so-called pinholes and microcracks, whose density is controlled by the surface quality of the polymer substrate. In addition, Rochat et al.[5] show that a source of coating defects includes the presence of inorganic additives in the superficial layers of the polymer substrate, such as antiblock particles. These additives protrude on the polymer surface and increase the coating roughness. They are therefore viewed as likely to affect the coating microstructure in the early stages of the deposition process.

In the present work, two different scales of defects were also evidenced in the aluminum coatings (Fig. 8). Although their sizes are very different, following the literature they were called macro defects (>1 µm) and microdefects (<1 µm).

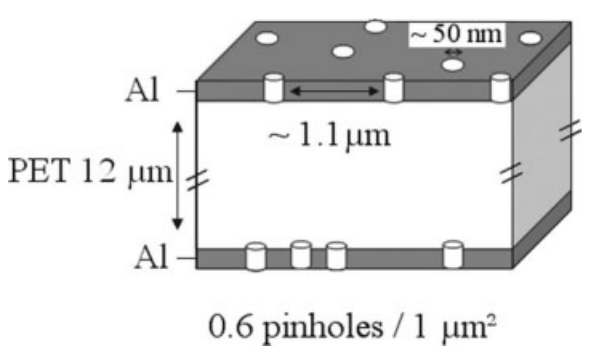

Figure 9 Order of magnitude of the heterogeneities present on the metallic layer of PETM2F400 film.

A global estimation on order of magnitude of pinholes present on the metallic layer has been established for PETM2F400 film (Fig. 9). Typical size of pinholes was close to 50 nm and average distance between defects was about 1.1 µm. In addition an average of 0.6 pinhole was measured in 1 µm^2. The schematic in Figure 9 show that the coated layer may not cooperate to improve the barrier properties of the film. In other words, the layers act independently because the thickness of the PET is much larger than the distance between neighboring defects, and no tortuosity parameter is needed to understand the data with several Al layers.

In addition, it appeared that the number of heterogeneities strongly depends on the aluminum thickness (Fig. 10). The number of pinholes is significantly reduced for the PET metallized on one side with 80 nm of aluminum, which is the sample with the highest aluminum content. Thornton[14,15] has shown that it is also a function of the local temperature and their time.

On the contrary, the size of pinholes decreased when the aluminum amount deposited on PET films was increased. Overall, the surface fraction occupied by pinholes linearly decreased with the aluminum thickness, Table III, Figure 10.

Influence of structural features on the physical properties of coated films

It has been suggested in the literature that the main mechanism for gases and water vapor transported through the multilayer structure was diffusion through coating defect, including pinholes, grain boundaries and microcracks.[16] Gases and water transport are not depended on the same effect.[1] In this section, both barrier and mechanical properties of aluminum coating deposited on PET films were investigated with particular attention paid to the

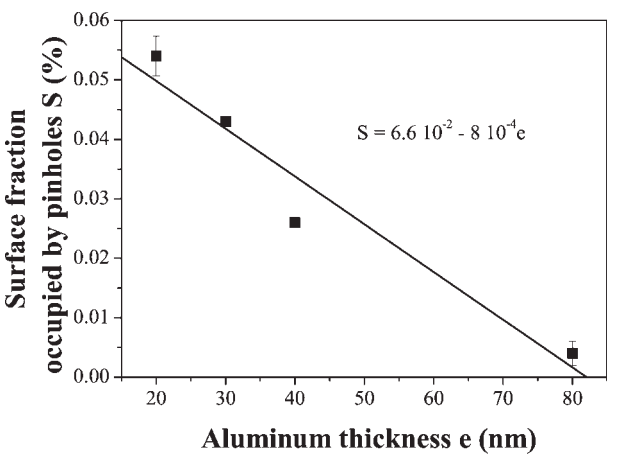

Figure 10 Dependence of fraction of the surface of pinholes on aluminum thickness.

TABLE III
Dependence of Fraction of the Surface of Pinholes on Aluminum Thickness

Films	Aluminum thickness (nm)	Area of pinholes/nm^2	Number of pinholes/μm^2	Surface fraction occupied by pinholes (%)
PETM1F200	20	240 ± 62	2.3 ± 0.5	0.054 ± 0.003
PETM1F300	30	140 ± 25	3.0 ± 0.3	0.043 ± 0.001
PETM1F400	40	62 ± 3.5	4.1 ± 0.6	0.026 ± 0.001
PETM1F800	80	57 ± 30	0.7 ± 0.7	0.004 ± 0.002

effect of structural features, mainly aluminum thickness and pinholes located in the metallic layers.

Mechanical properties

Typical stress–strain curves from tensile tests ($n = 5$) on PET films are shown Figure 11. Investigated materials exhibit a rather ductile behavior with strains at elastic yielding between 2.8% (TD) and 3.1% (MD). For PET yield stress mean values of 84 and 96 MPa were obtained in TD and MD, respectively. For slow velocity, the direction dependence is small due to relaxation. The 12 μm PET film exhibits the best values for stress at fracture in MD while the best values for strain at fracture were demonstrated for PET in TD. A similar behavior is evidenced for the coated materials. In addition, experimental results on PET films show that the values of yield stress increase with crosshead speed.

Figure 12 shows the influence of structural features on tensile energy to fracture. The tensile energy to fracture values are in the range 7–11 kJ/m^3. The variation is not clearly significant because it is in the range of the standard deviation measured for a given type of samples. The conclusion of these measurements is that the mechanical properties of the films are very similar despite the different aluminum thicknesses. In addition, an increase of the surface fraction occupied by pinholes does not degrade significantly the mechanical properties of PET films. The latter observation seems in disagreement with the literature.[17] To better asses the influence of surface holes on the mechanical properties, the essential work to fracture method is a more discriminating tool.[18]

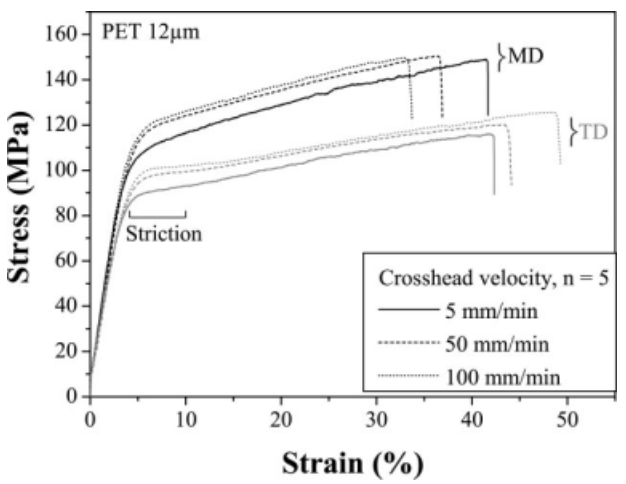

Figure 11 Stress versus strain curves ($n = 5$), the figure presents the most representative example). Experimental results for PET reference film at initial state, in the machine and transverse directions (MD and TD) and for different crosshead velocity.

Permeability

The amount of water vapor permeating through the film results in an increase in the moisture content of the gas flowing. The permeability constants obtained in the case of the base PET films are in good

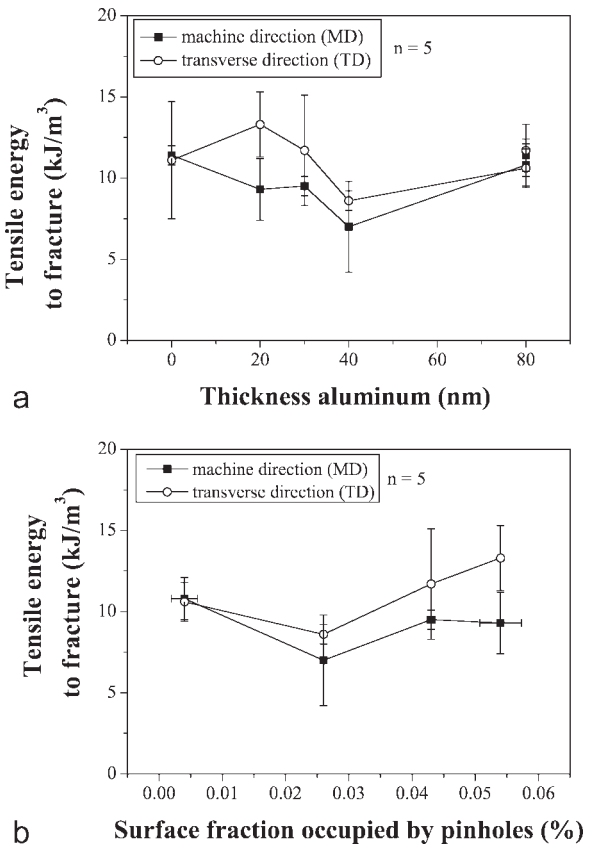

Figure 12 Variation of the tensile energy to fracture with (a) aluminum thickness and (b) surface fraction occupied by pinholes.

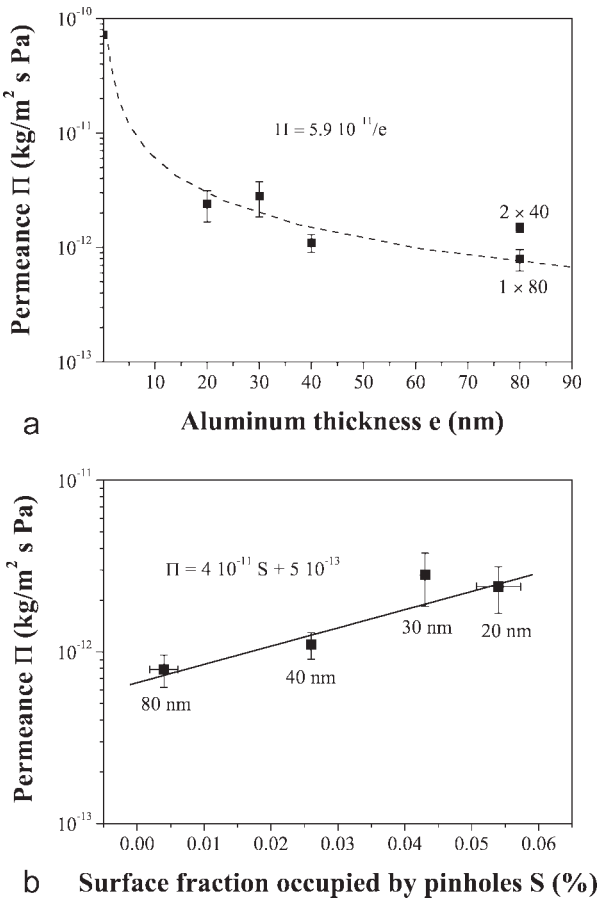

Figure 13 Variation of the permeance with (a) aluminum thickness and (b) fraction of the surface of pinholes. The number shown on the top of the point is the corresponding aluminum thickness for polymer-metal films.

agreement with the literature. Jeon et al.[19] indicate a vapor flow value of 22 g/(m^2 day) for a 25 μm PET film at 36°C, 90% RH. Our experimental results lead to a mean value for the 12 μm neat PET of 17.7 ± 0.2 g/(m^2 day) at 25°C, 90%RH. When divided by film thickness, deviation between theses two values is of about 40%.

The dependence of the permeation rate on the coating thickness of barrier coated polymer has already been discussed.[4] Most data reviewed by Chatham show an initial strong decrease in oxygen permeation rate when a barrier layer is applied and increased in thickness. In the case of water vapor permeability, it can be observed that the permeability depend significantly on the aluminum thickness (Fig. 13). The permeance of 12 μm thick PET substrate was reduced by about a factor of 30 after applying a 20 nm thick layer of aluminum; the permeance values are of 7.2 × 10^{-11} kg/m^2 s Pa and 2.4 × 10^{-12} kg/m^2 s Pa for PET and PET metallized on one side with 20 nm of aluminum, respectively.

Figure 13(a) shows a strong decrease of permeance with aluminum thickness to about 40 nm, then a

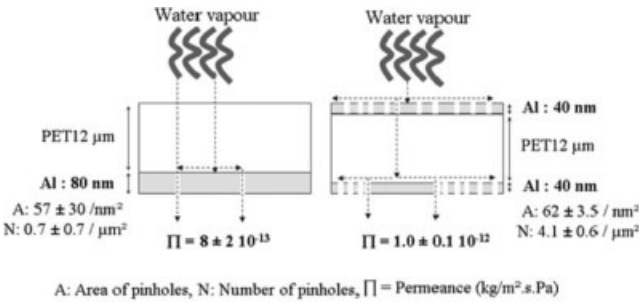

Figure 14 Schematic representation of the sideways diffusion mechanism water vapor transfer through pinholes for a sample with one and two barrier layers.

constant residual permeation is observed. The literature[3] report that a residual permeation exist even when the barrier inorganic coatings are relatively thick (=70 nm); Sobrinho et al.[3] attribute this phenomenon to the presence of microscopic defects in the SiO_2 or SiN coatings. Bonnebat[20] indicates a residual permeation to water vapor [~1.2 × 10^{-9} kg/(m^2 s)] for PET metallized with aluminum for an optical density (OD) of 3.5 which corresponds to 54 nm. According to the results presented in,[21] Figure 13(b) shows that the permeance linearlly increases with surface fraction occupied by pinholes in the considered range of surface fraction. PETM1F800 (Al:1 × 80 nm) and PETM2F400 (Al:2 × 40 nm) products basically showed similar barrier properties. Previously discussed results have shown that surface fraction occupied by pinholes for PETM1F400 was six times higher than that of PETM1F800 (Fig. 10). As described earlier, this result may not be the consequence of a purely geometrical effect. A double metallization with 40 nm aluminum layer was expected to be more efficient than only one 80 nm aluminum layer because of a specific mechanism[9] implying the border and that would be named sideway mechanism in which the transport

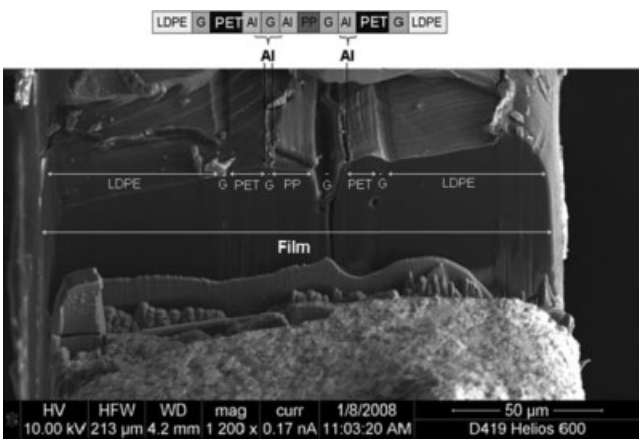

Figure 15 Thickness aluminum determinated by FIB technic.

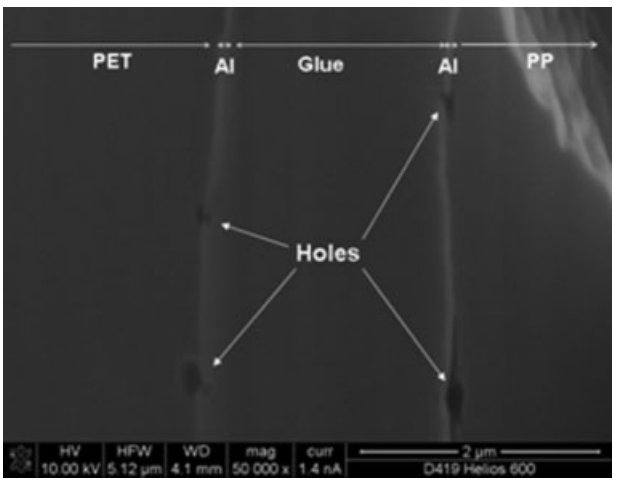

Figure 16 Holes in polymer-aluminum layers interface which could be filled by glue.

of water vapor is favored in the direction of the film surface (Fig. 14).

TOWARD A COMMERCIAL PRODUCT

From the analysis of the experimental results, it has been shown that defect population of the coating significantly influences the barrier properties of the coated system. This is known for O_2 and N_2, but not for water, where thickness only was called to be important.[1] So, the permeation mechanism for inorganic barrier films on polymer substrates will be usually dominated by defects in the inorganic barrier film. To obtain more information about the defects and their possible origins in multilayers, SEM examinations were performed on cross section of commercial product obtained by ion beam milling. The complex shown in Figure 15 is constituted of ten layers: LDPE (60 µm)/glue (2 µm)/PET (12 µm)/Al (0.040 µm)/glue (2 µm)/Al (0.040 µm)/PP (20 µm)/glue (2 µm)/Al (0.040 µm)/PET (12 µm)/glue (2 µm)/LDPE (60 µm). The brighter layer is aluminum and the darker ones are PET or glue.

Two main types of defects were identified, namely:

i. Holes in polymer-aluminum layers interface which could be filled by glue (Fig. 16)
ii. A fracture of thin aluminum layer (Fig. 17)

In addition, in some occurrences, regularly spaced holes in the aluminum layer are observed as shown in Figure 18 such a feature suggest multiple cracking. There is a fracture visible in the lower left part on this figure. The regular distance between hole might have occurred during the strain needed for this fracturing.

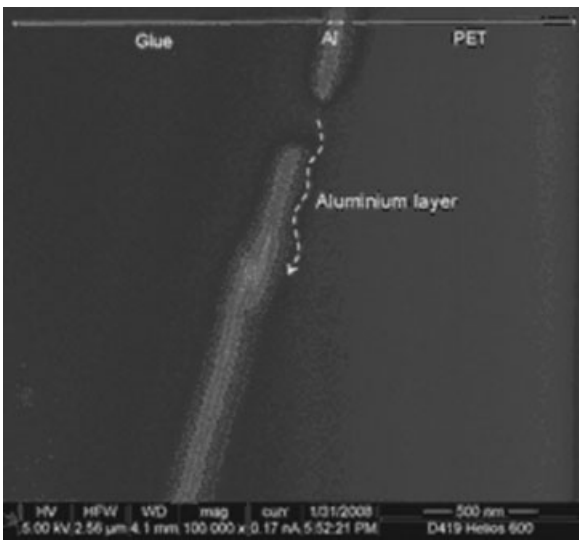

Figure 17 Fracture of thin aluminum layer.

According to previous studies, disruptions in the aluminum layer under stress generated by mechanical stress could be probably due to the production process.[11,16,20,22] Thornton and Hoffman[23] have been showed that virtually all vacuum-deposited coatings are in a state of stress (a thermal stress and an intrinsic stress) and that the diffusion processes can cause flaws such as holes and hillocks to form. Brunner et al.[11] indicate that this kind of disruption is also found at sites where interface impurities between the aluminum layer and its substrate exist. In addition, it is likely that this impurity was already present before the metallization process despite the foregoing plasma cleaning.

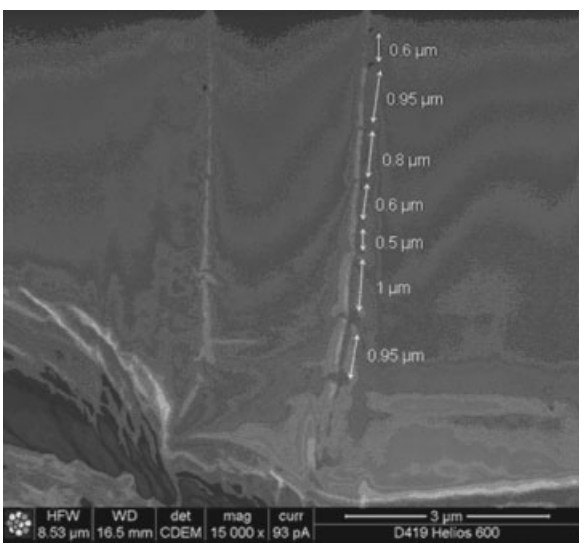

Figure 18 Regularity of the average distance between holes.

CONCLUSION

Pinholes were observed in the aluminum layer of metallized composites. An average of 0.6 pinhole was measured in 1 μm^2 for a film metallized with 40 nm of aluminum on two sides; typical size of pinholes was close to 50 nm and average distance between defects was about 1.1 μm. It was shown that the surface occupied by pinholes linearly decreases with the aluminum thickness and that the permeance of water linearly increases with surface fraction occupied by pinholes in the considered range of surface fraction. A such correlation was before known for oxygen but not for water. Therefore, an exact knowledge of aluminum thickness deposited on substrate is required to produce films with the desired barrier performance. Electrical measurement is an efficient tool to make a quality control during or after the film's fabrication.

A multilayer commercial product was analyzed to better understand how the defects could be formed. Two types of defects were identified: (i) holes in polymer-aluminum layers interface which could be filled by glue, (ii) a fracture of thin aluminum layer probably generates by production process.

Beside the mentioned efficient electrical measurements, light passing through was also named to be a good and affordable method for checking the amount of pinholes at this production step.[24]

The authors thank Francine Roussel-Dherbey of CMTC, Consortium des Moyens Technologiques Communs (38, France), Frédéric Delabrouille and Emmanuelle Pons of EDF for their important contributions to the SEM analyzes.

References

1. IEA Annex 39 "High Performance Thermal Insulation in Building and Building Systems," final report. 2005. Available at www.vip-bau.ch.
2. Simmler, H.; Brunner, S. Energy Build 2005, 37, 1122.
3. Da Silva Sobrinho, A.; Czeremuszkin, G.; Latrèche, M.; Dennler, G.; Wertheimer, M. Surf Coat Technol 1999, 116, 1204.
4. Chatham, H. Surf Coat Technol 1996, 78, 1.
5. Rochat, G.; Leterrier, Y.; Fayet, P.; Mansona, J. Surf Coat Technol 2005, 200, 2236.
6. Rasband, W. ImageJ is a free processing software developed at National Institutes of Health, NIH, 1997.
7. Mohney, S. E.; Wang, B.; Cabassi, M. A.; Lew, K. K.; Dey, S.; Redwing, J. M.; Mayer, T. S. Solid-State Electron 2005, 49, 227.
8. Vargel, C. Tech Ing 1999, 4661, 1.
9. Maspoch, M.; Hénault, D.; Velasco, J.; Santana, O. Polym Test 2000, 19, 559.
10. Norme "Produits isolants thermiques destinés aux applications du bâtiment" NF EN 12086. November 1997, p 75-215.
11. Brunner, S.; Gasser, P.; Simmler, H.; Wakili, K. Surf Coat Technol 2006, 200, 5908.
12. Singh, B.; Bouchet, J.; Rochat, G.; Leterrier, Y.; Manson, J. A. E.; Fayet, P. Surf Coat Technol 2007, 201, 7107.
13. Roberts, A. P.; Henry, B. M.; Sutton, A. P.; Grovenor, C. R. M.; Briggs, G. A. D.; Miyamoto, T.; Kano, M.; Tsukahara, Y.; Yanaka, M. J. Membr Sci 2002, 208, 75.
14. Thornton, J. A. J. Vac Sci Technol 1974, 11, 666.
15. Thornton, J. A. J Vac Sci Technol 1986, 4, 6.
16. Hedenqvist, M.; Johanson, K. Surf Coat Technol 2003, 172, 7.
17. Cros, B.; Vallat, M.; Despaux, G. Appl Surf Sci 1998, 126, 159.
18. Garnier, G.; Chehab, B.; Yrieix, B.; Bréchet, Y.; Flandin, L. J Mat Sci 2009.
19. Jeon, D. H.; Lee, K. H.; Park, H. J. Radiat Phys Chem 2004, 71, 1059.
20. Bonnebat, C. Journée Spécialisée CACEMI, France, J.S04-06 CNAM. 2004, 1-34.
21. Garnier, G. PhD thesis, INPGrenoble, 2009.
22. Sugiyama, A.; Tada, H.; Yoshimoto, M. Vuoto 1999, 1.
23. Thornton, J. A.; Hoffman, D. W. Thin Solid Films 1989, 171, 5.
24. Garnier, G.; Bréchet, Y.; Flandin, L. J Mat Sci 2009, 44, 4692.